

MiR-483 induces senescence of human adipose-derived mesenchymal stem cells through *IGF1* inhibition

Junyan Shen¹, Xiaoqi Zhu¹, Hailiang Liu¹

¹Institute for Regenerative Medicine, Shanghai East Hospital, Tongji University School of Medicine, Shanghai 200123, China

Correspondence to: Hailiang Liu; email: hailiang_1111@tongji.edu.cn

Keywords: mesenchymal stem cell, senescence, adipogenesis

Received: October 18, 2019

Accepted: July 6, 2020

Published: August 15, 2020

Copyright: Shen et al. This is an open-access article distributed under the terms of the Creative Commons Attribution License (CC BY 3.0), which permits unrestricted use, distribution, and reproduction in any medium, provided the original author and source are credited.

ABSTRACT

Human adipose-derived mesenchymal stem cells (hADSCs) are an ideal source of seed cells for regenerative applications and tissue engineering. However, long-term *in vitro* culture of hADSCs reduces their quantity and quality, which lessens their value in research and clinical applications. The molecular mechanisms underlying this biological process are poorly defined. Recently identified microRNAs (miRNAs) have emerged as critical modulators of cellular senescence. In this study, we examined the changes in hADSCs undergoing senescence. Significant miR-483-3p upregulation was noted during *in vitro* passaging of hADSCs, which correlated with the adipogenic differentiation and cellular senescence. Knockdown of miR-483-3p retarded the adipogenic differentiation potential of hADSCs and reduced cellular senescence. Dual-luciferase reporter assays identified insulin-like growth factor-1 (*IGF1*) as the target gene of miR-483-3p. *IGF1* inhibition confirmed its inhibitory effects on replicative senescence in hADSCs. In conclusion, our study revealed essential regulatory roles of miR-483-3p in the adipogenesis and aging of hADSCs mediated by targeting *IGF1*.

INTRODUCTION

Mesenchymal stem cells (MSCs) are a type of stem cells that can be isolated from adipose tissues, bone marrow, and umbilical cord blood [1]. Recent studies have shown that MSCs can be used as pluripotent stem cells to repair damaged tissues, produce biologically active molecules to promote tissue regeneration and regulate the maturation and function of innate and adaptive immune effector cells [2, 3]. These features make MSCs ideal candidates for cell-based therapy of many diseases. Human adipose-derived mesenchymal stem cells (hADSCs) can easily be isolated and have strong differentiation and proliferation abilities *in vitro*, and have thus become the ultimate source of seed cells for regenerative applications and tissue engineering. However, long-term culture of MSCs results in altered cell morphology, slower proliferation rates and variations in differentiation potential [4, 5].

There is substantial evidence that the aging of MSCs contributes to age-related diseases and aging, and that replicative senescence damages the regenerative potential of MSCs [6]. It is crucial to understand the mechanisms that lead to replicative senescence in MSCs to evaluate potential approaches to maintaining their regenerative function and thereby produce more robust regenerative cells for cellular therapy.

MicroRNAs (miRNAs) are endogenous single-stranded RNAs composed of 19–25 nucleotides and regulate the expression of their complementary messenger RNAs (mRNAs) [7, 8]. Regulation by miRNAs leads to mRNA destruction or translational repression of target genes [9]. Previous studies have demonstrated that miRNAs play essential roles in various cellular and biological processes, including cell apoptosis, cell proliferation, cancer, and metabolic diseases [10–12].

In recent studies, miRNAs have emerged as modulators of the expression of genes associated with cellular senescence [13]. MiR-483 gene family is first discovered as part of intron 2 of insulin-like growth factor-2 (*IGF2*) [14]. MiR-483 suppresses chondrogenic differentiation of hMSCs [15]. However, the potential effects of miR-483 on the replicative senescence of hADSCs are obscure.

In this study, we investigated the following changes in hADSCs undergoing senescence: increased ability of adipogenic differentiation, shortened telomere length, enhanced activity of the acidic senescence-associated β -galactosidase (SA- β -gal), and increased expression of p16, p21, and p53. We demonstrated that knockdown of miR-483-3p inhibited aging-related adipogenic differentiation of hADSCs. Insulin-like growth factor-1 (*IGF1*) was identified as a target gene of miR-483-3p. We also discovered that miR-483-3p expression was markedly increased during senescence of hADSCs cultured *in vitro*. Ultimately, we identified miR-483-3p as a novel, direct molecular regulator involved in the replicative senescence of hADSCs.

RESULTS

Characterization and verification of senescent MSCs

The senescence phenotypes of hADSCs grown *in vitro* were assessed by isolating hADSCs from two different donors and subjecting to long-term proliferation under the same culture conditions. After passage 9 (P9), hADSCs gradually increased in size, and acquired a flat and irregular shape, which is the typical morphology of senescent cells (Supplementary Figure 1A, 1B). Flow cytometry analysis showed that hADSCs from early (P9) and late (P16) passages were both positive for the MSCs surface markers CD73, CD90, and CD105, but negative for CD34, CD45, CD11b, CD19 and HLA-DR (Supplementary Figure 1C, 1D).

Another key criterion for the identification of MSCs is their potential to differentiate into osteoblasts and adipocytes. Here, we analyzed the effect of replicative senescence on the differentiation potential of hADSCs. Our findings revealed that hADSCs undergoing long-term culture had an increased adipocyte differentiation ability but a reduced osteocyte differentiation ability (Figure 1A, 1B).

Furthermore, the expression of three cell senescence-related molecular markers (p16, p21, and p53) were significantly increased from P9 to P16 (Figure 1C). Additionally, the number of cells that positively stained with SA- β -gal was significantly increased in P16 (Figure 1D). Cell counting kit-8 (CCK-8) assay results

showed that the proliferation of hADSCs was significantly downregulated in P16 (Figure 1E). Changes in telomere length were evaluated using quantitative PCR (qPCR) [16], which revealed that telomere shortening occurred during the aging of hADSCs *in vitro* (Figure 1F). These data generally indicated that hADSCs exhibit a constant increase in senescence with successive passaging in culture.

MiRNAs expression in the adipogenic differentiation of hADSCs

Previous studies have revealed that osteoblasts and adipocytes share a common mesenchymal ancestor and that the distinct processes of osteogenic and adipogenic differentiation from MSCs are competitive [17]. We found that adipogenic differentiation of hADSCs increased during cellular senescence which was consistent with previous findings [18]. Comparative sequencing of small RNA using adipogenic differentiation samples from day 0 (undifferentiated) and day 14 were performed to identify any putative miRNAs that simultaneously affect adipogenic differentiation and replicative senescence in hADSCs (Figure 2A, 2B).

Apart from miR-1908, which has been reported to be highly expressed during adipogenic differentiation of hADSCs [19], we found that miR-483-3p and miR-483-5p expression were also significantly increased during adipogenesis (Figure 2C). To further verify these results, miR-483-5p and miR-483-3p expression were analyzed using RT-qPCR (Figure 2D, 2E). As pre-miR-483 is located in intron 2 of the *IGF2* transcript and encodes two mature miRNAs (miR-483-3p/miR-483-5p) (Figure 2F), and *IGF2* modulates the differentiation of stem cells [20, 21], we also measured the *IGF2* expression using RT-qPCR. Consistently, *IGF2* and miR-483 displayed similar expression pattern in adipogenic differentiated hADSCs that were isolated from two different donors and cultured under the same conditions (Supplementary Figure 2). Therefore, we speculated that miR-483 plays a vital role in the differentiation of hADSCs.

MiR-483 promotes adipogenesis of hADSCs *in vitro*

To further investigate the role of miR-483 in the differentiation of hADSCs, we transfected hADSCs with 483-3p-I (an inhibitor of miR-483-3p), 483-5p-I (an inhibitor of miR-483-5p), or negative control inhibitor (I-CT). The transfection efficiency was quantified at 48 hours after transfection by RT-qPCR. The success of the inhibition was demonstrated by low miR-483-5p and miR-483-3p expression (Figure 3A, 3B). We induced adipogenic differentiation of hADSCs

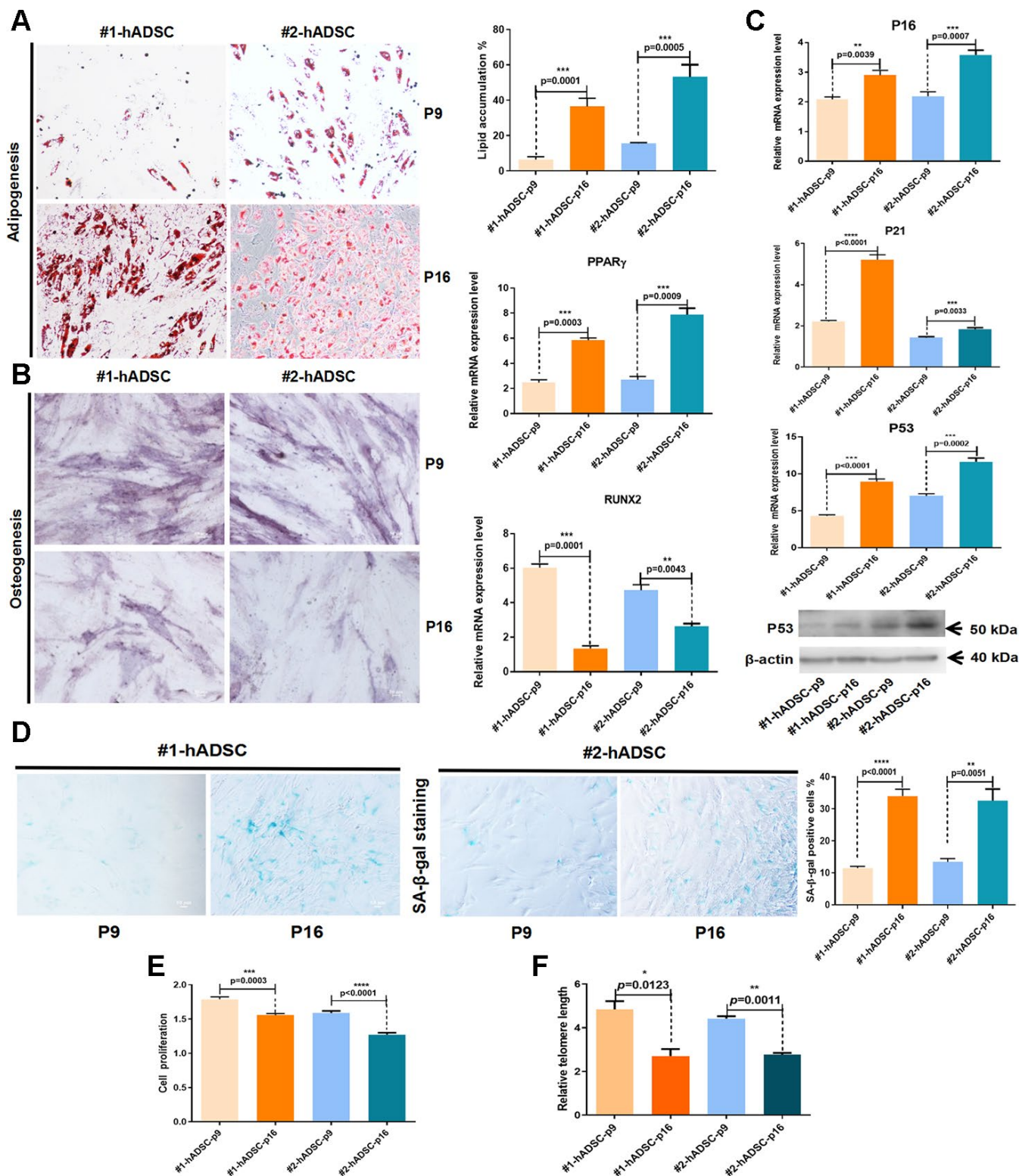


Figure 1. Characterization and verification of senescent MSCs from human adipose tissues from two different donors (#1 and #2). (A) Oil Red O staining of hADSCs at P9 and P16 (10 \times ; scale: 50 μ m); MRNA expression of PPAR γ was evaluated by RT-qPCR. (B) Alkaline phosphatase staining of hADSCs at P9 and P16 (10 \times ; scale: 50 μ m); MRNA expression of RUNX2 was evaluated by RT-qPCR. (C) MRNA expression levels of p16, p21, and p53 were evaluated by RT-qPCR; western blot analysis of p53. (D) SA- β -gal staining of hADSCs at P9 and P16 (10 \times ; scale: 50 μ m). (E) The proliferation of hADSCs at P9 and P16 was detected by CCK-8 assay. (F) Telomere length was demonstrated by qPCR.

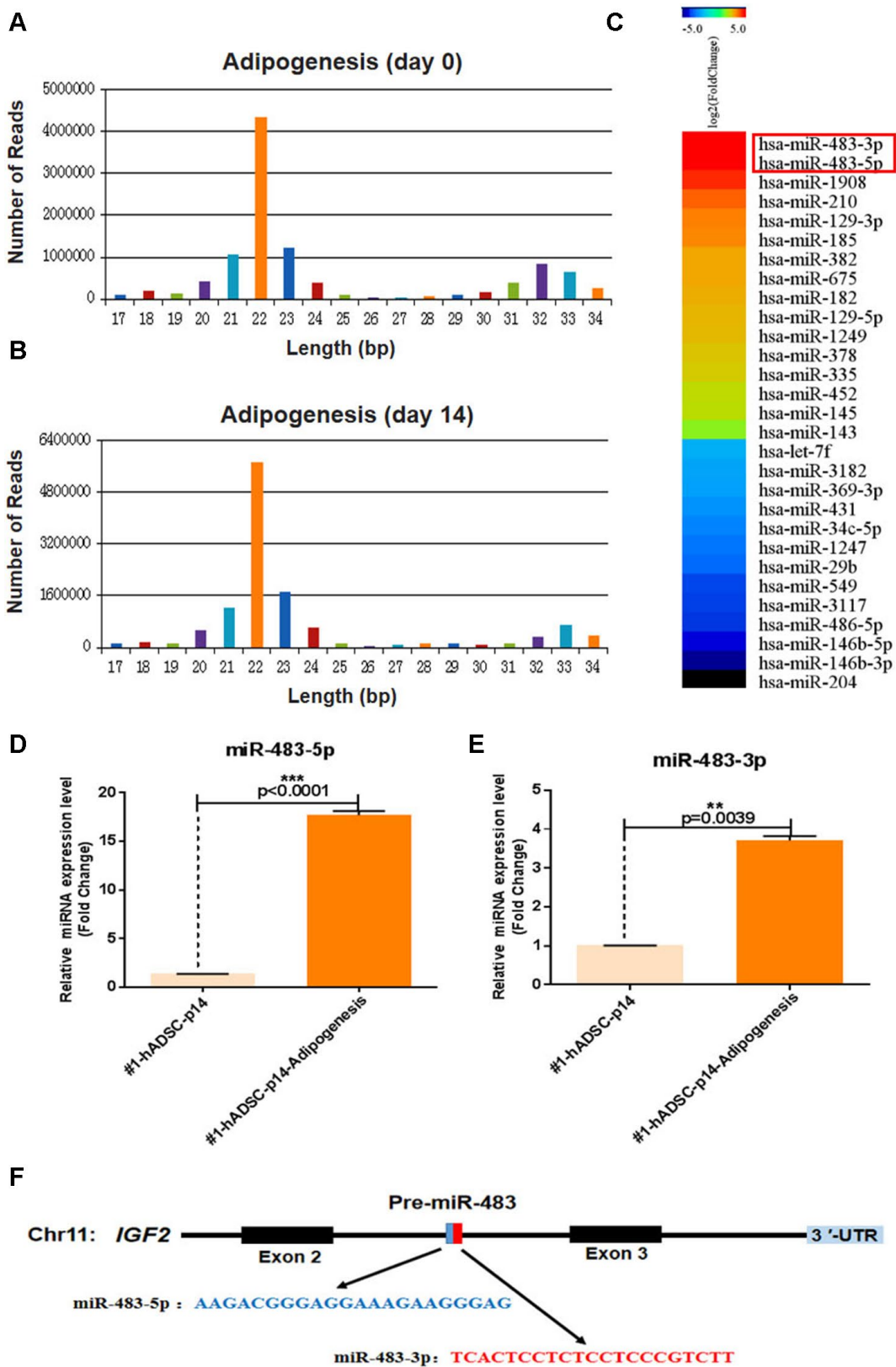


Figure 2. MiR-483 expression during the adipogenic differentiation of hADSCs. (A, B) Small-RNA sequencing was performed to profile miRNAs with variant expression during adipogenic differentiation of hADSCs. Data are expressed as the number of reads and (C) differentially expressed miRNA genes. (D, E) The relative expression of miR-483-5p and miR-483-3p was validated by RT-qPCR. (F) The location and classification of miR-483.

transfected with 483-5p-I, 483-3p-I, or I-CT, then measured the adipogenic induction efficacy. It was found that inhibition of miR-483-5p and miR-483-3p in hADSCs decreased the number of lipid droplets (Figure 3C). To confirm these results, we investigated the expression of two primary adipogenic transcription factors, lipoprotein lipase (*LPL*) and peroxisome proliferator-activated receptor-gamma (*PPAR* γ), by RT-qPCR (Figure 3D, 3E) and western blot analysis (Figure 3F). Compared with the control group, the mRNA and protein levels of *LPL* and *PPAR* γ were significantly decreased in the 483-3p-I group, but not in the 483-5p-I group. Because miR-483-3p had the stronger effect of the two miRNAs, we selected it for further characterization.

MiR-483-3p directly targets the 3'UTR of *IGF1* mRNA

The biological process underlying the regulation of adipogenesis by miR-483-3p was further illustrated by the bioinformatics analysis of potential miR-483-3p target genes using the TargetScanHuman 7.0 and miRWalk online databases. Through database prediction, we selected *IGF1*, O-linked N-acetylglucosamine transferase (*OGT*), and chloride voltage-gated channel (*CLCN3*) as potential targets of miR-483-3p. We cloned the 3' UTRs of these three genes separately into a dual-luciferase-based

reporter plasmid and cloned miR-483-3p into pSUPER. The miR-483-3p plasmid or control plasmid was then co-transfected with one of the three reporter plasmids into HEK-293T cells. While the presence of miR-483-3p significantly decreased the luciferase reporter activity of *IGF1*, the decreases in the activities of *OGT* and *CLCN3* were not significant (Supplementary Figure 3). We also created a mutation of eight nucleotides within the mRNA binding site of miR-483-3p to interrupt the hypothetical connection between the *IGF1* mRNA and miR-483-3p (Figure 4A, 4B). As shown in Figure 4B, the mutant miR-483-3p restored the luciferase activity of *IGF1*.

HADSCs were also transfected with 483-3p-I or 483-3p-M (mimic of miR-483-3p), and RT-qPCR was used to quantify the mRNA levels of *IGF1*. *IGF1* expression was downregulated by miR-483-3p overexpression (Figure 4C) and upregulated by miR-483-3p inhibition (Figure 4D). These observations generally suggested that *IGF1* is a direct target gene of miR-483-3p.

MiR-483-3p induces senescence of hADSCs through *IGF1*

Given that miR-483-3p was upregulated during adipogenic differentiation and that it controlled the expression of adipogenic differentiation markers and phenotypes, we sought to determine whether it was

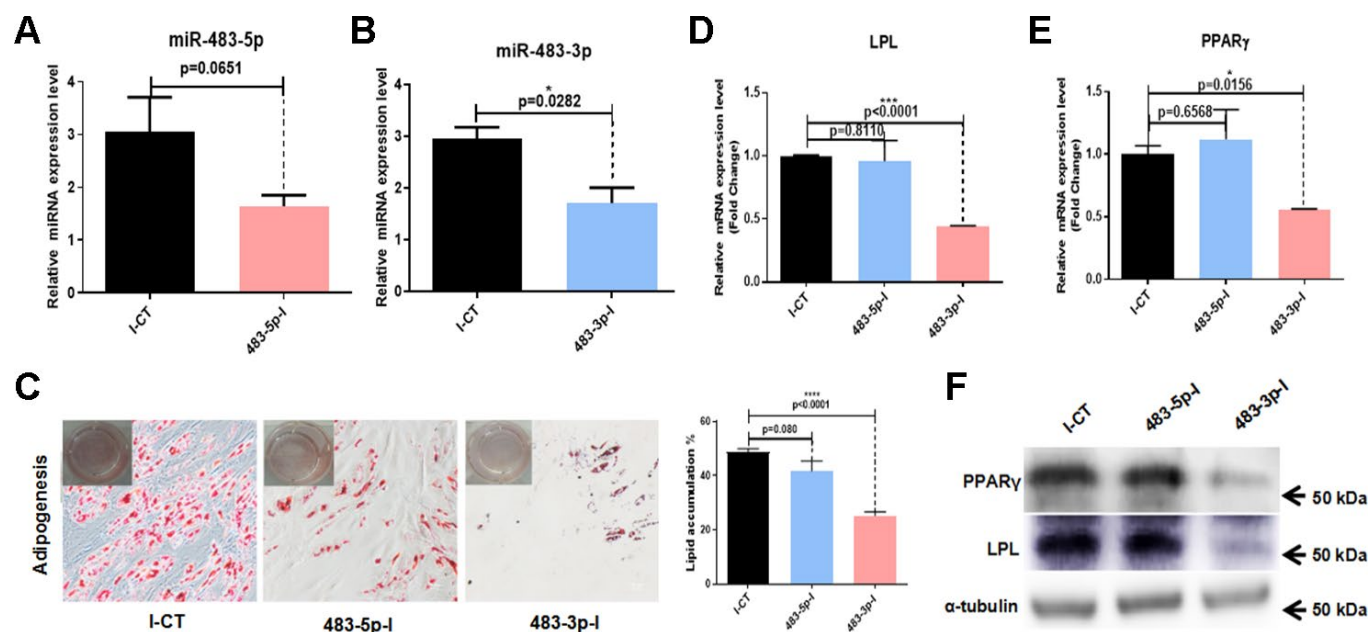


Figure 3. Effects of miR-483 on adipogenic differentiation of hADSCs. (A, B) The efficiency of miR-483-5p and miR-483-3p inhibition was assayed by RT-qPCR. (C) The effect of inhibition of miR-483-3p and miR-483-5p on adipogenic differentiation of hADSCs was evaluated on day 14 using Oil Red O staining (10 \times ; scale: 50 μ m). (D–F) RT-qPCR and western blot analysis of *LPL* and *PPAR* γ expression levels. I-CT: negative control inhibitor; 483-5p-I: inhibitor of miR-483-5p; 483-3p-I: inhibitor of miR-483-3p.

involved in hADSC senescence *in vitro*. The expression levels of miR-483-3p during early and late passages of hADSCs taken from two different donor samples were examined using RT-qPCR. MiR-483-3p expression was significantly increased in senescent cells (Figure 5A). To further investigate the biological effect of miR-483-3p on hADSC senescence phenotypes, hADSCs were transfected with 483-3p-I or 483-3p-M to alter the *in vitro* expression levels of miR-483-3p, then stained for SA- β -gal. Transfection with 483-3p-M increased the activity of SA- β -gal while 483-3p-I decreased it compared with the corresponding control group (Figure 5B, 5C). Interestingly, we also found that *IGF1* expression was significantly reduced in senescent cells (Figure 5D).

Based on these results, we transfected hADSCs with the small interfering RNA (siRNA) si-*IGF1* to inhibit endogenous *IGF1* expression. The results of RT-qPCR and ELISA showed that si-*IGF1* effectively reduced *IGF1* expression (Figure 5E, 5F). Additionally, the SA- β -gal activity of the si-*IGF1* transfection group was significantly higher than that of the si-NC group (Figure 5G).

To further verify the relationship between miR-483-3p and *IGF1* in the *in vitro* aging of hADSCs, we co-transfected hADSCs with 483-3p-I and si-*IGF1*. The

knockdown of miR-483-3p reduced SA- β -gal activity, but the additional transfection of si-*IGF1* restored this activity in hADSCs compared with the control group (Figure 5H).

DISCUSSION

The high abundance of hADSCs makes them the ideal source of adult stem cells in clinical and regenerative medicine. However, long-term culture of mesenchymal stem cells (MSCs) results in altered cell morphology, slower proliferation rates, and disruption of the balance between osteogenesis and adipogenesis [4, 5]. In our study, MSCs undergoing long-term proliferation displayed a significant increase in senescence, as evidenced by their shortened telomere length and increased expression of SA- β -gal, p16, p21, and p53. These results concur with the findings of previous studies [22, 23].

While many studies have focused on the potential of aging MSCs to undergo adipogenic and osteogenic differentiation, several of these studies have reported conflicting findings. Most studies have reported that MSCs undergoing long-term culture exhibit a decline in all differentiation abilities, but the results of some

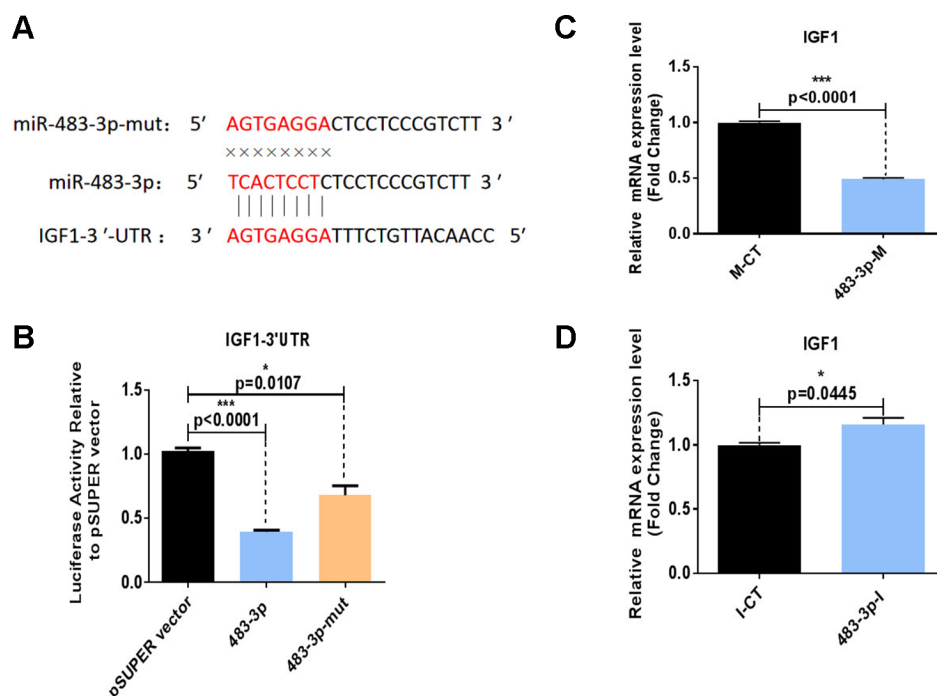


Figure 4. Identification of *IGF1* as a direct target of miR-483-3p. (A) Putative miR-483-3p target sites in *IGF1* and design of mutation sites. (B) Activity of the luciferase reporter gene in HEK-293T cells co-transfected with a luciferase reporter plasmid containing *IGF1* 3' UTRs and wild-type pSUPER-miR-483-3p, mutant pSUPER-miR-483-3p, or empty pSUPER vector. Luciferase activity was assayed 32 hours after transfection. (C, D) RT-qPCR analysis of *IGF1* mRNA levels in hADSCs transfected with 483-3p-M or 483-3p-I. mut: mutant; M-CT: mimic control; 483-3p-M: mimic of miR-483-3p.

studies have suggested the opposite [24, 25]. Lei et al. demonstrated that the osteogenic potential decreased during replicative senescence in MSCs, while the adipogenic potential increased in late passages [18]. Likewise, the results of our study indicated that the osteogenic differentiation potential decreases as the adipogenic differentiation potential increases in late passages. However, the mechanism of this phenomenon remains unknown.

Accumulating evidence suggests that miRNAs induce mRNA degradation and translational repression to regulate various cellular processes, such as proliferation, apoptosis, and differentiation [26]. Motoi et al. reported that miR-195 was highly expressed in old MSCs, which directly inactivated telomerase reverse transcriptase (TERT) and facilitated the senescence of MSCs, and abrogation of miR-195 could reverse stem cell senescence [27]. Another study by Wang et al.

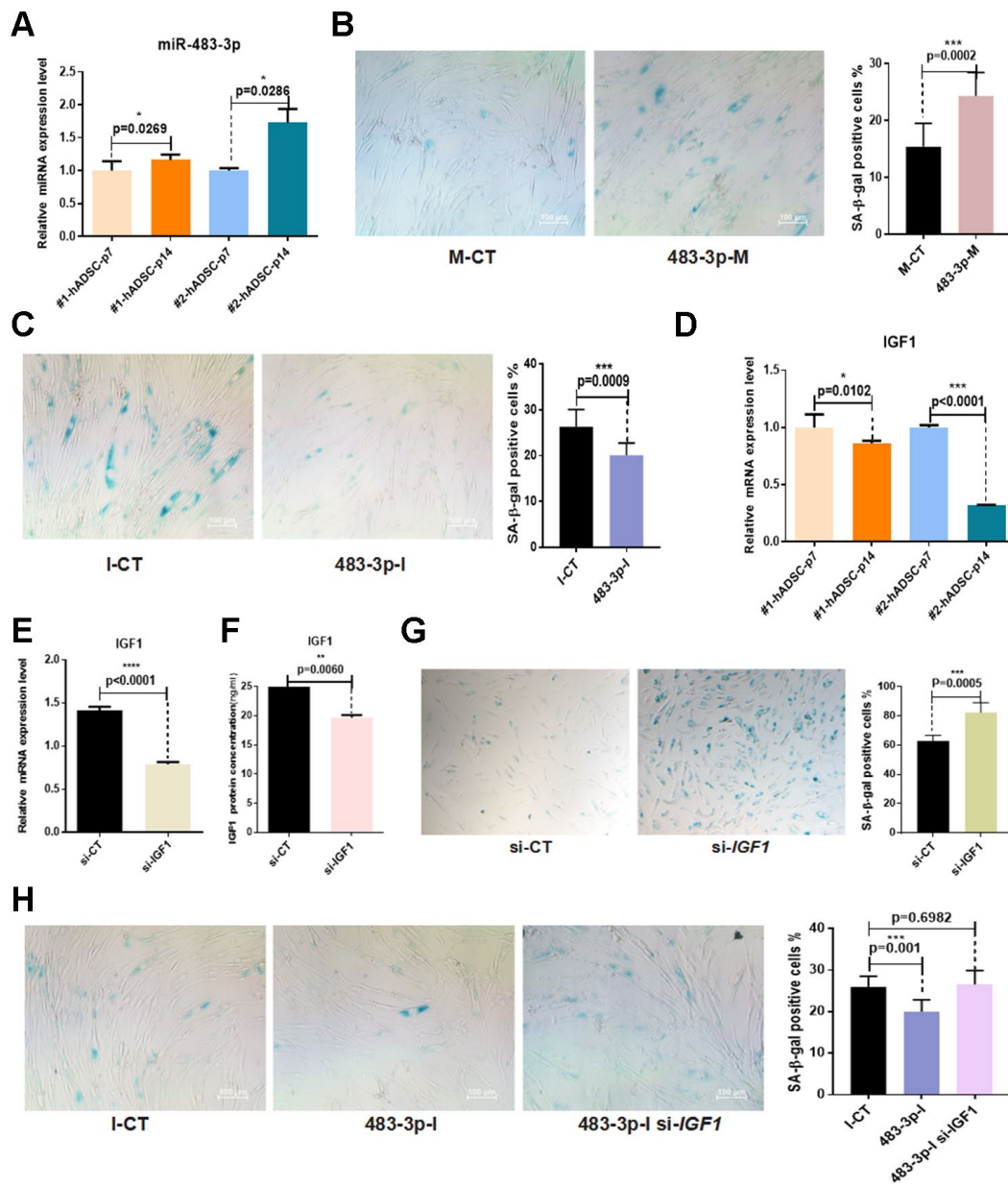


Figure 5. Effects of miR-483-3p and IGF1 on senescence of hADSCs. (A) MiR-483-3p expression at early-passage (P7) and late-passage (P14) hADSCs was detected by RT-qPCR. (B) SA-β-gal staining of hADSCs (P14) transfected with 483-3p-M and corresponding control (10×; scale: 100μm). (C) SA-β-gal staining of hADSCs (P14) transfected with 483-3p-I and corresponding control (10×; scale: 100μm). (D) IGF1 expression in hADSCs at P7 and P14 was detected by RT-qPCR. (E, F) Efficiency of IGF1 inhibition was assayed by RT-qPCR and ELISA. (G) SA-β-gal staining of hADSCs (P14) transfected with si-CT or si-IGF1 (4×; scale: 100μm). (H) SA-β-gal staining of hADSCs (P14) co-transfected with 483-3p-I and si-IGF1 (10×; scale: 100μm).

showed that miR-26b-3p was drastically upregulated during continuous *in vitro* passaging of human umbilical cord-derived MSCs, and played a vital role in regulating their proliferation [28].

Replicative senescence is a process marked by continuous, cumulative changes, and the resultant “aging phenotype” of hADSCs becomes more obvious with successive passaging. Accordingly, we chose late passage hADSCs to identify potential miRNAs that exert crucial functions during adipogenic differentiation and replicative senescence of hADSCs. MiR-483-3p expression was significantly upregulated during the adipogenic differentiation, and miR-483-3p inhibition limited the adipogenic potential of hADSCs. To elucidate the molecular mechanisms by which miR-483-3p regulates adipogenic differentiation, we performed the bioinformatics analysis of potential miR-483-3p target genes using the online databases. Notably, bioinformatics analysis and experimental data confirmed that *IGF1* is a direct target of miR-483-3p. In addition, there was a negative correlation between *IGF1* and miR-483-3p expression at the protein and mRNA levels in hADSCs.

IGF1, a primary hormone of growth and fat metabolism, is known to work through the binding of insulin-like growth factor receptor. The complex effects of IGF1 on normal growth and survival have been extensively studied, and while some research articles offer insightful observations, they also highlight paradoxes. The use of calorie restriction to inhibit IGF1 and mTOR has been widely demonstrated as an efficient anti-aging strategy because it was the most effective inducer of autophagy [29, 30]. However, an inactive form of *IGF1* results in severe growth retardation and proliferative defects in mice [31, 32]. IGF1 is considered to be the most potent growth factor for the prevention of apoptosis in eukaryotic cells [33]. Several prospective studies investigated the role of IGF1 in promoting PI3K/AKT signaling, which promotes cell proliferation and inhibits cell senescence [34–36]. IGF1 also regulates the proliferation and self-renewal of stem cells [37], and plays an essential role in skeletal development by promoting proliferation and osteogenic differentiation of MSCs [38].

Previous research has demonstrated that miR-483 is widely involved in a variety of cancers through the inhibition of proliferation, invasion and migration, and the induction of apoptosis [39–41]. Until this study, the effect of miR-483-3p on the replicative senescence of hADSCs remains unclear. We investigated that miR-483-3p was highly expressed, while *IGF1* mRNA was expressed at a low level in late-passage hADSCs. The knockdown of miR-483-3p inhibited the senescence of

hADSCs, while simultaneous knockdown of *IGF1* restored the effect of miR-483-3p.

There are some drawbacks and limitations to our study. Firstly, miR-483 is located in intron 2 of *IGF2* and we found that miR-483 and *IGF2* have similar expression pattern in adipogenic differentiated hADSCs. However, our study only demonstrated the effects of miR-483-3p on hADSCs, further investigations of *IGF2* were needed. Secondly, although miR-483-3p was involved in replicative senescence of hADSCs, its exact role remains inconclusive. The questions of whether miR-483-3p plays a substantial role in aging and whether miR-483-3p inhibition can reverse the development of aging *in vivo* must be addressed in future studies.

In conclusion, we identified miR-483-3p as a key promoter of adipogenesis and a vital player in the regulation of replicative senescence in hADSCs through *IGF1* inhibition. MiR-483-3p also appears to be a novel indicator of replicative senescence in hADSCs. These findings provide essential clues for manipulating *IGF1* via miR-483-3p to attenuate aging and promote the proliferation of hADSCs.

MATERIALS AND METHODS

Isolation and characterization of hADSCs

Samples of subcutaneous adipose tissues were obtained from patients without malignant tumors, autoimmune diseases, congenital diseases, or genetic diseases, at the age of 30 (#1) and 34 (#2) undergoing fracture surgery. The operation protocols were approved by the Ethics Research Committee, Tongji University School of Medicine.

Tissue was excised from blood vessels and sliced into approximately 1 mm³ size, digested in a 0.2% collagenase type I/II mixture (Gibco, New York, USA) at 37°C for 1 hour, filtered with 70- μ m nylon mesh and then subjected to centrifugation at 1,500 rpm for 10 minutes. The cells were cultured in DMEM/F12 medium supplemented with 10% fetal bovine serum, 1% non-essential amino acids, 100 U/mL penicillin and 100 μ g/mL streptomycin, in a 5% CO₂ environment at 37°C. After one week of culture when the cells reached about 80% confluence, they were passaged and transferred one-third of cells to a new culture dish (passage 1, P1). At P2, surface antigen sorting was performed on adherent and spindle-shaped hADSCs according to the following criteria: positive for CD73, CD90, and CD105 and negative for CD34, CD45, CD11b, CD19 and HLA-DR (BD, Human MSC Analysis Kit). Adipogenic and osteogenic differentiation kits (Gibco, New York, USA) were used

to induce adipogenesis and osteogenesis, respectively. The adipocyte phenotype was evaluated using Oil Red O staining according to the previously described protocols [23]. Osteoblast phenotype was assessed using BCIP/NBT Alkaline Phosphatase staining assay kit according to the manufacturer's protocols (Beyotime, Shanghai, China).

Cell proliferation CCK-8 assay

Cell proliferation ability was evaluated using CCK-8 assay (Dojindo, Shanghai, China) in early-passage and late-passage hADSCs according to the manufacturer's instructions. Briefly, cells were cultured in 96-well plates at a concentration of 1×10^4 cells/well. After 24 hours of culture, 10 μ L CCK-8 reagent was added to each well and further incubated for 4 hours. The absorbance was determined at a wavelength of 450nm using SpectraMax M5 (Molecular Devices, CA, USA).

MiRNAs sequencing

The miRNAs samples were extracted using the mirVana™ miRNA Isolation Kit (Ambion, Waltham, USA) following the manufacturer's instructions. Small RNA libraries were prepared using the Small RNA Sample Preparation kit (Illumina, San Diego, USA) according to the manufacturer's protocols. The quality of the purified small RNA sequencing libraries was confirmed on an Agilent 2100 Bioanalyzer. The small RNA sequencing data were first cleaned using small RNA sequencing data cleaning pipeline. Next, the clean sequence data were aligned to miRBase to detect and estimate the expression of microRNAs. Subsequently, the remaining read sequences were aligned to the fRNAdb to get the expression of various non-coding RNAs. The miRNAs sequencing data generated in this study have been deposited in the NCBI Gene Expression Omnibus (GEO) under accession number GSE138879.

Cell transfection

Mimics of miR-483-3p (483-3p-M) and miR-483-5p (483-5p-M), inhibitors of miR-483-3p (483-3p-I), and their corresponding negative controls (mimic-NC (M-CT) and inhibitor-NC (I-CT)), and the siRNA of *IGF1* (si-*IGF1*) and its corresponding negative control (si-NC) were synthesized by Genepharma (Shanghai, China). hADSCs were grown until 50%–60% confluence then transfected with 100 nM miRNA mimic, inhibitor or NC using Lipofectamine 2000 reagent (Invitrogen, CA, USA). The culture medium was changed after 12 hours of transfection and cellular differentiation was induced 48 hours later according to the manufacturer's recommendations.

Dual-luciferase reporter assay

A partial sequence of *IGF1* containing the predicted miR-483-3p binding site was amplified by PCR and cloned into the dual-luciferase plasmid. The miR-483-3p gene and a mutant 'seed' sequence were synthesized by Thermo Fisher Scientific and cloned into the pSUPER vector. Reporter assays were performed in HEK-293T cells, which were harvested 32 hours after transfection. Firefly and Renilla luciferase activities were measured using the Dual-Glo Luciferase assay system (Promega, Madison, USA). A signal from the green Renilla luciferase intracellular protein was normalized to the red firefly luciferase signal.

RT-qPCR analysis

Total RNA was extracted using Trizol reagent (Invitrogen, California, USA). The quality and concentration of total RNA were determined using a nanodrop 2000 and separation on a 1% agarose gel. Reverse transcription and detection of miRNAs were accomplished using the all-in-one miRNA qRT-PCR detection kit (Genecopoeia, Maryland, USA) according to the manufacturer's instructions. mRNA expression was quantified via an initial synthesis of cDNA using a PrimeScript RT reagent kit (Takara, Dalian, China), followed by RT-qPCR using SYBR Green SuperMix (Bio-Rad, California, USA) on the Quantstudio 7 Flex Real-Time PCR system (Thermo Scientific, MA, USA). Each sample was tested in triplicate. The relative expression levels of miRNAs and mRNA were normalized to the expression of U6 and β -actin, respectively. The relative gene expression was calculated using the comparative CT ($2^{-\Delta\Delta CT}$) method, and the sequences of the primers used were listed in Table 1.

Western blot analysis

Cells were washed twice with cold phosphate-buffered saline, then lysed with RIPA lysis buffer containing protease inhibitor and shaken for 15 minutes on ice. Protein samples were subjected to centrifugation at 12,000 \times g for 15 minutes, and the supernatants were collected. Protein concentration was determined using bicinchoninic acid protein assay kit (Beyotime). Samples containing equal amounts of protein were separated by sodium dodecyl sulfate-polyacrylamide gel electrophoresis and then transferred onto a 0.22- μ m polyvinylidene difluoride membrane. After blocking with 5% non-fat milk (Sigma, St. Louis, USA), the membranes were incubated with a primary antibody (PPAR γ : ab191407, Abcam, Cambridge, UK; LPL: ab172953, Abcam; α -tubulin: T9026, Sigma) at 4°C overnight, then further incubated with the

Table 1. Primer sequences used in this study.

| Target gene | Forward primer (5'--3') | Reverse primer (5'--3') |
|---------------|---|---|
| β-actin | F: ACCCACACTGTGCCCATCT | R: ATGTCACGCACGATTCC |
| p16 | F: TTCCTGGACACGCTGGT | R: GGTTACTGCCTCTGGTGC |
| p21 | F: TTAGCAGCGGAACAAGGA | R: AAGACAACACTCCCAGCCC |
| p53 | F: TGCATTTTCACCCACCCCTT | R: ACACAGGTGGCAGCAAAGTT |
| IGF1 | F: ATGCTCTTCAGTTCGTGTGTGG | R:CAATACATCTCCAGCCTCCTTAGA |
| IGF2 | F: GCTGGCAGAGGAGTGTCC | R: AGGTGAGAAGCACCAGCATC |
| TEL | F:GGTTTTTGAGGGTGAGGGTGAGGGTGAGGG TGAGGGT | R:TCCCGACTATCCCTATCCCTATCCCTATCCCTA TCCCTA |
| 36B4 | F: CAGCAAGTGGGAAGGTGTAATCC | R:CCCATTCTATCATCAACGGGTACAA |
| LPL | F:CTGGACGGTAACAGGAATGTATGAG | R: CATCAGGAGAAAGACGACTCGG |
| PPAR γ | F: CCTATTGACCCAGAAAGCGATT | R: CATTACGGAGAGATCCACGGA |
| RUNX2 | F:TGTCATGGCGGGTAACGAT | R:AAGACGGTTATGGTCAAGGTGAA |
| miR-483-3p | F:TCACTCCTCTCCTCCCGTCTT | |
| miR-483-5p | F:AAGACGGGAGGAAAGAAGGGAG | |
| U6 | F:GCTTCGGCAGCACATATACTAAAAT | |

Note: F: forward; R: reverse; TEL: Telomere DNA sequence

corresponding secondary antibody (170-6515 and 170-6516, Bio-Rad) according to the manufacturer's instructions. Protein bands were quantified using the Amersham Imager system.

Assay of cellular senescence (SA-β-gal staining)

Cells were cultured in 24-well plates at a concentration of 2×10^4 cells/well. SA-β-gal activity was determined using the Cell Senescence β-Galactosidase Staining Kit (Beyotime) according to the manufacturer's instructions. The nuclei were stained with DAPI, and blue-stained senescent cells were counted using Image J.

ELISA

The protein content of IGF1 in cells was determined using the Human IGF1 enzyme-linked immunosorbent assay (ELISA) kit (Elabscience, Wuhan, China) according to the manufacturer's instructions.

Statistical analysis

Results are expressed as the means \pm standard deviation ($n=3$). Student's t-test was used to determine significance between two groups. A P-value <0.05 was considered statistically significant.

Abbreviations

hADSCs: Human adipose-derived mesenchymal stem cells; miRNAs: microRNAs; SA-β-gal: senescence-associated β-galactosidase; IGF1: insulin-like growth factor-1; MSCs: Mesenchymal stem cells; mRNAs: messenger RNAs; IGF2: insulin-like growth factor-2; 3' UTR: 3' untranslated region; CCK-8: Cell counting

kit-8; RT-qPCR: real-time quantitative PCR; LPL: lipoprotein lipase; PPAR γ : peroxisome proliferator-activated receptor gamma; OGT: O-linked N-acetylglucosamine transferase; CLCN3: chloride voltage-gated channel; siRNA: small interfering RNA; TERT: telomerase reverse transcriptase.

AUTHOR CONTRIBUTIONS

L.H.L. designed the study; S.J.Y. and Z.X.Q. performed and drafted the experiment; L.H.L. performed miRNA-seq data analyses; L.H.L. revised the manuscript; L.H.L. supervised the entire project; and all authors approved the final version of the manuscript.

CONFLICTS OF INTEREST

All authors declare that no conflicts of interest exist.

FUNDING

This work was supported by grants from the National Key Research and Development Program (2020YFC2002800), National Natural Science Foundation of China (Grant No 31671539, 31370214), and Major Program of the Development Fund for Shanghai Zhangjiang National Innovation Demonstration Zone (Stem Cell Strategic Biobank and Stem Cell Clinical Technology Transformation Platform) (ZJ2018-ZD-004).

REFERENCES

1. Chang YH, Liu HW, Wu KC, Ding DC. Mesenchymal Stem Cells and Their Clinical Applications in Osteoarthritis. Cell transplantation. 2016; 25:937–950.

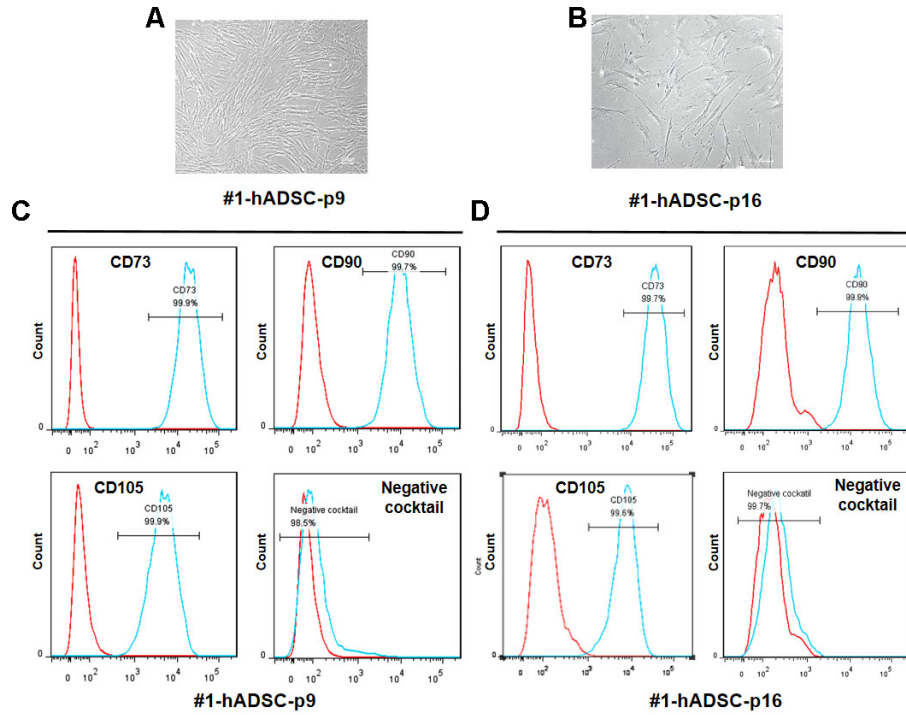
- <https://doi.org/10.3727/096368915X690288>
PMID:26688464
2. Li N, Hua J. Interactions between mesenchymal stem cells and the immune system. *Cell Mol Life Sci.* 2017; 74:2345–60.
<https://doi.org/10.1007/s00018-017-2473-5>
PMID:28214990
 3. Wong SP, Rowley JE, Redpath AN, Tilman JD, Fellous TG, Johnson JR. Pericytes, mesenchymal stem cells and their contributions to tissue repair. *Pharmacol Ther.* 2015; 151:107–20.
<https://doi.org/10.1016/j.pharmthera.2015.03.006>
PMID:25827580
 4. Wagner W, Bork S, Lepperdinger G, Joussem S, Ma N, Strunk D, Koch C. How to track cellular aging of mesenchymal stromal cells? *Aging (Albany NY).* 2010; 2:224–30.
<https://doi.org/10.18632/aging.100136>
PMID:20453259
 5. Baker N, Boyette LB, Tuan RS. Characterization of bone marrow-derived mesenchymal stem cells in aging. *Bone.* 2015; 70:37–47.
<https://doi.org/10.1016/j.bone.2014.10.014>
PMID:25445445
 6. Turinetti V, Vitale E, Giachino C. Senescence in human mesenchymal stem cells: functional changes and implications in stem cell-based therapy. *Int J Mol Sci.* 2016; 17:1164.
<https://doi.org/10.3390/ijms17071164>
PMID:27447618
 7. Ambros V, Bartel B, Bartel DP, Burge CB, Carrington JC, Chen X, Dreyfuss G, Eddy SR, Griffiths-Jones S, Marshall M, Matzke M, Ruvkun G, Tuschl T. A uniform system for microRNA annotation. *RNA.* 2003; 9:277–79.
<https://doi.org/10.1261/rna.2183803>
PMID:12592000
 8. Bartel DP. MicroRNAs: genomics, biogenesis, mechanism, and function. *Cell.* 2004; 116:281–97.
[https://doi.org/10.1016/s0092-8674\(04\)00045-5](https://doi.org/10.1016/s0092-8674(04)00045-5)
PMID:14744438
 9. Mohr AM, Mott JL. Overview of microRNA biology. *Semin Liver Dis.* 2015; 35:3–11.
<https://doi.org/10.1055/s-0034-1397344>
PMID:25632930
 10. Cullen BR. Transcription and processing of human microRNA precursors. *Mol Cell.* 2004; 16:861–65.
<https://doi.org/10.1016/j.molcel.2004.12.002>
PMID:15610730
 11. Qadir MI, Faheem A. miRNA: a diagnostic and therapeutic tool for pancreatic cancer. *Crit Rev Eukaryot Gene Expr.* 2017; 27:197–204.
<https://doi.org/10.1615/CritRevEukaryotGeneExpr.2017.0197>
PMID:29199604
 12. Price NL, Ramírez CM, Fernández-Hernando C. Relevance of microRNA in metabolic diseases. *Crit Rev Clin Lab Sci.* 2014; 51:305–20.
<https://doi.org/10.3109/10408363.2014.937522>
PMID:25034902
 13. Choi SW, Lee JY, Kang KS. miRNAs in stem cell aging and age-related disease. *Mech Ageing Dev.* 2017; 168:20–29.
<https://doi.org/10.1016/j.mad.2017.08.013>
PMID:28847486
 14. Liu M, Roth A, Yu M, Morris R, Bersani F, Rivera MN, Lu J, Shioda T, Vasudevan S, Ramaswamy S, Maheswaran S, Diederichs S, Haber DA. The IGF2 intronic miR-483 selectively enhances transcription from IGF2 fetal promoters and enhances tumorigenesis. *Genes Dev.* 2013; 27:2543–48.
<https://doi.org/10.1101/gad.224170.113>
PMID:24298054
 15. Anderson BA, McAlinden A. miR-483 targets SMAD4 to suppress chondrogenic differentiation of human mesenchymal stem cells. *J Orthop Res.* 2017; 35:2369–77.
<https://doi.org/10.1002/jor.23552> PMID:28244607
 16. Cawthon RM. Telomere measurement by quantitative PCR. *Nucleic Acids Res.* 2002; 30:e47.
<https://doi.org/10.1093/nar/30.10.e47>
PMID:12000852
 17. Chen Q, Shou P, Zheng C, Jiang M, Cao G, Yang Q, Cao J, Xie N, Velletri T, Zhang X, Xu C, Zhang L, Yang H, et al. Fate decision of mesenchymal stem cells: adipocytes or osteoblasts? *Cell Death Differ.* 2016; 23:1128–39.
<https://doi.org/10.1038/cdd.2015.168> PMID:26868907
 18. Lei Q, Liu T, Gao F, Xie H, Sun L, Zhao A, Ren W, Guo H, Zhang L, Wang H, Chen Z, Guo AY, Li Q. Microvesicles as potential biomarkers for the identification of senescence in human mesenchymal stem cells. *Theranostics.* 2017; 7:2673–89.
<https://doi.org/10.7150/thno.18915>
PMID:28819455
 19. Yang L, Shi CM, Chen L, Pang LX, Xu GF, Gu N, Zhu LJ, Guo XR, Ni YH, Ji CB. The biological effects of hsa-miR-1908 in human adipocytes. *Mol Biol Rep.* 2015; 42:927–35.
<https://doi.org/10.1007/s11033-014-3830-1>
PMID:25421647
 20. Bergman D, Halje M, Nordin M, Engström W. Insulin-like growth factor 2 in development and disease: a mini-review. *Gerontology.* 2013; 59:240–49.
<https://doi.org/10.1159/000343995>
PMID:23257688

21. Diao S, Yang H, Cao Y, Yang D, Fan Z. IGF2 enhanced the osteo-/dentinogenic and neurogenic differentiation potentials of stem cells from apical papilla. *J Oral Rehabil.* 2019. [Epub ahead of print]. <https://doi.org/10.1111/joor.12859> PMID:[31291686](https://pubmed.ncbi.nlm.nih.gov/31291686/)
22. Kim J, Kim Y, Choi H, Kwon A, Jekarl DW, Lee S, Jang W, Chae H, Kim JR, Kim JM, Kim M. Ubiquitin C decrement plays a pivotal role in replicative senescence of bone marrow mesenchymal stromal cells. *Cell Death Dis.* 2018; 9:139. <https://doi.org/10.1038/s41419-017-0032-5> PMID:[29382826](https://pubmed.ncbi.nlm.nih.gov/29382826/)
23. Park JS, Kim HY, Kim HW, Chae GN, Oh HT, Park JY, Shim H, Seo M, Shin EY, Kim EG, Park SC, Kwak SJ. Increased caveolin-1, a cause for the declined adipogenic potential of senescent human mesenchymal stem cells. *Mech Ageing Dev.* 2005; 126:551–59. <https://doi.org/10.1016/j.mad.2004.11.014> PMID:[15811424](https://pubmed.ncbi.nlm.nih.gov/15811424/)
24. Bonab MM, Alimoghaddam K, Talebian F, Ghaffari SH, Ghavamzadeh A, Nikbin B. Aging of mesenchymal stem cell in vitro. *BMC Cell Biol.* 2006; 7:14. <https://doi.org/10.1186/1471-2121-7-14> PMID:[16529651](https://pubmed.ncbi.nlm.nih.gov/16529651/)
25. Wagner W, Horn P, Castoldi M, Diehlmann A, Bork S, Saffrich R, Benes V, Blake J, Pfister S, Eckstein V, Ho AD. Replicative senescence of mesenchymal stem cells: a continuous and organized process. *PLoS One.* 2008; 3:e2213. <https://doi.org/10.1371/journal.pone.0002213> PMID:[18493317](https://pubmed.ncbi.nlm.nih.gov/18493317/)
26. Tomé M, López-Romero P, Albo C, Sepúlveda JC, Fernández-Gutiérrez B, Dopazo A, Bernad A, González MA. miR-335 orchestrates cell proliferation, migration and differentiation in human mesenchymal stem cells. *Cell Death Differ.* 2011; 18:985–95. <https://doi.org/10.1038/cdd.2010.167> PMID:[21164520](https://pubmed.ncbi.nlm.nih.gov/21164520/)
27. Okada M, Kim HW, Matsu-ura K, Wang YG, Xu M, Ashraf M. Abrogation of age-induced MicroRNA-195 rejuvenates the senescent mesenchymal stem cells by reactivating telomerase. *Stem Cells.* 2016; 34:148–59. <https://doi.org/10.1002/stem.2211> PMID:[26390028](https://pubmed.ncbi.nlm.nih.gov/26390028/)
28. Wang Q, Xu C, Zhao Y, Xu Z, Zhang Y, Jiang J, Yan B, Gu D, Wu M, Wang Y, Liu H. miR-26b-3p regulates human umbilical cord-derived mesenchymal stem cell proliferation by targeting estrogen receptor. *Stem Cells Dev.* 2016; 25:415–26. <https://doi.org/10.1089/scd.2015.0267> PMID:[26723394](https://pubmed.ncbi.nlm.nih.gov/26723394/)
29. Barzilay N, Huffman DM, Muzumdar RH, Bartke A. The critical role of metabolic pathways in aging. *Diabetes.* 2012; 61:1315–22. <https://doi.org/10.2337/db11-1300> PMID:[22618766](https://pubmed.ncbi.nlm.nih.gov/22618766/)
30. Johnson SC. Nutrient sensing, signaling and ageing: the role of IGF-1 and mTOR in ageing and age-related disease. *Subcell Biochem.* 2018; 90:49–97. https://doi.org/10.1007/978-981-13-2835-0_3 PMID:[30779006](https://pubmed.ncbi.nlm.nih.gov/30779006/)
31. Liu JP, Baker J, Perkins AS, Robertson EJ, Efstratiadis A. Mice carrying null mutations of the genes encoding insulin-like growth factor I (Igf-1) and type 1 IGF receptor (Igf1r). *Cell.* 1993; 75:59–72. PMID:[8402901](https://pubmed.ncbi.nlm.nih.gov/8402901/)
32. Powell-Braxton L, Hollingshead P, Warburton C, Dowd M, Pitts-Meek S, Dalton D, Gillett N, Stewart TA. IGF-I is required for normal embryonic growth in mice. *Genes Dev.* 1993; 7:2609–17. <https://doi.org/10.1101/gad.7.12b.2609> PMID:[8276243](https://pubmed.ncbi.nlm.nih.gov/8276243/)
33. Bianchi VE, Locatelli V, Rizzi L. Neurotrophic and neuroregenerative effects of GH/IGF1. *Int J Mol Sci.* 2017; 18:2441. <https://doi.org/10.3390/ijms18112441> PMID:[29149058](https://pubmed.ncbi.nlm.nih.gov/29149058/)
34. Ma X, Xu W, Zhang Z, Liu N, Yang J, Wang M, Wang Y. Salvianolic acid B ameliorates cognitive deficits through IGF-1/Akt pathway in rats with vascular dementia. *Cell Physiol Biochem.* 2017; 43:1381–91. <https://doi.org/10.1159/000481849> PMID:[28992623](https://pubmed.ncbi.nlm.nih.gov/28992623/)
35. Zhou W, Wang J, Qi Q, Feng Z, Huang B, Chen A, Zhang D, Li W, Zhang Q, Bjerkgvig R, Li X, Wang J. Matrine induces senescence of human glioblastoma cells through suppression of the IGF1/PI3K/AKT/p27 signaling pathway. *Cancer Med.* 2018; 7:4729–43. <https://doi.org/10.1002/cam4.1720> PMID:[30079478](https://pubmed.ncbi.nlm.nih.gov/30079478/)
36. Luo X, Jiang X, Li J, Bai Y, Li Z, Wei P, Sun S, Liang Y, Han S, Li X, Zhang B. Insulin-like growth factor-1 attenuates oxidative stress-induced hepatocyte premature senescence in liver fibrogenesis via regulating nuclear p53-progerin interaction. *Cell Death Dis.* 2019; 10:451. <https://doi.org/10.1038/s41419-019-1670-6> PMID:[31171766](https://pubmed.ncbi.nlm.nih.gov/31171766/)
37. Bendall SC, Stewart MH, Menendez P, George D, Vijayaragavan K, Werbowetski-Ogilvie T, Ramos-Mejia V, Rouleau A, Yang J, Bossé M, Lajoie G, Bhatia M. IGF and FGF cooperatively establish the regulatory stem cell niche of pluripotent human cells in vitro. *Nature.* 2007; 448:1015–21. <https://doi.org/10.1038/nature06027> PMID:[17625568](https://pubmed.ncbi.nlm.nih.gov/17625568/)
38. Chen CY, Tseng KY, Lai YL, Chen YS, Lin FH, Lin S. Overexpression of insulin-like growth factor 1

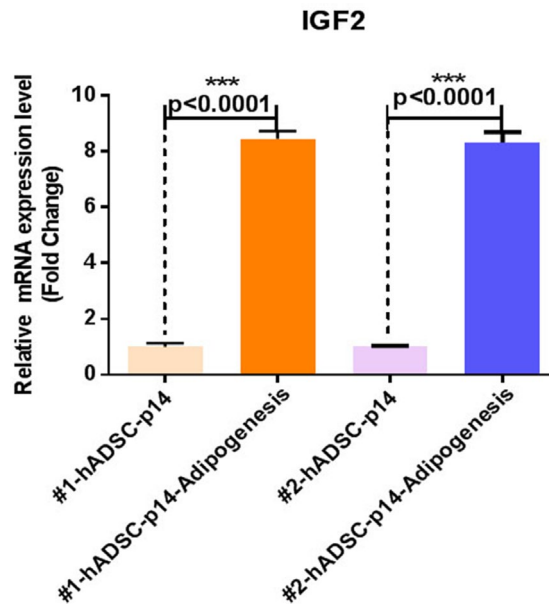
- enhanced the osteogenic capability of aging bone marrow mesenchymal stem cells. *Theranostics*. 2017; 7:1598–611.
<https://doi.org/10.7150/thno.16637> PMID:[28529639](https://pubmed.ncbi.nlm.nih.gov/28529639/)
39. Yu FY, Zhou CY, Liu YB, Wang B, Mao L, Li Y. miR-483 is down-regulated in gastric cancer and suppresses cell proliferation, invasion and protein O-GlcNAcylation by targeting OGT. *Neoplasma*. 2018; 65:406–14.
https://doi.org/10.4149/neo_2018_170608N411
PMID:[29788742](https://pubmed.ncbi.nlm.nih.gov/29788742/)
40. Niu ZY, Li WL, Jiang DL, Li YS, Xie XJ. Mir-483 inhibits colon cancer cell proliferation and migration by targeting TRAF1. *Kaohsiung J Med Sci*. 2018; 34:479–86.
<https://doi.org/10.1016/j.kjms.2018.04.005>
PMID:[30173777](https://pubmed.ncbi.nlm.nih.gov/30173777/)
41. Xiang Y, Song Y, Li Y, Zhao D, Ma L, Tan L. miR-483 is down-regulated in polycystic ovarian syndrome and inhibits KGN cell proliferation via targeting insulin-like growth factor 1 (IGF1). *Med Sci Monit*. 2016; 22:3383–93.
<https://doi.org/10.12659/msm.897301>
PMID:[27662007](https://pubmed.ncbi.nlm.nih.gov/27662007/)

SUPPLEMENTARY MATERIALS

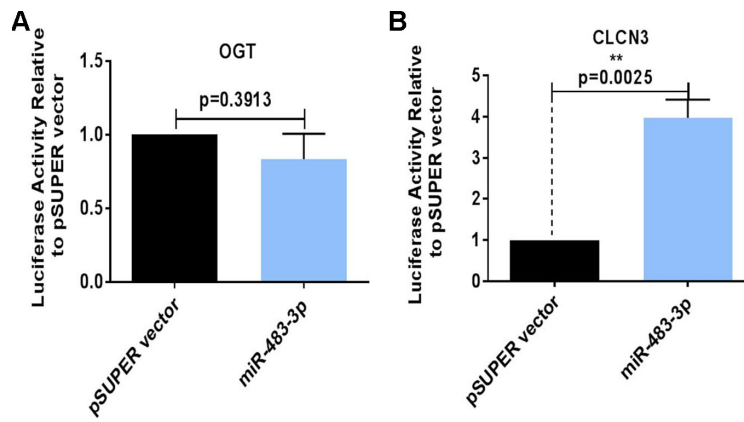
Supplementary Figures



Supplementary Figure 1. Senescence phenotype of hADSCs at different passages. (A, B) The morphology of donor #1 hADSCs was observed under a microscope at P9 and P16. (C, D) Immunophenotypic characterization of #1hADSCs at P9 and P16 by flow cytometry.



Supplementary Figure 2. IGF2 expression during adipogenic differentiation of hADSCs was analyzed by RT-qPCR.



Supplementary Figure 3. Luciferase reporter assay analysis of miR-483 potential target genes. (A, B) Luciferase reporter activity in HEK-293T cells co-transfected with the luciferase reporter plasmid containing *OGT* and *CLCN3* 3'UTRs and wild-type pSUPER-miR-483-3p or empty pSUPER vector. Luciferase activity was assayed 32 hours after transfection.